PERGAMON

International Journal of Heat and Mass Transfer 45 (2002) 509–518

International Journal of HEAT and MASS TRANSFER

www.elsevier.com/locate/ijhmt

A new mathematical method to solve highly coupled equations of heat and mass transfer in porous media

N. Mendes [a,*], P.C. Philippi [b], R. Lamberts [b]

[a] *Department of Mechanical Engineering, Pontifical Catholic University of Paraná, Rua Imaculada Conceição, 1155 Prado Velho, Curitiba, PR, 80215-901, Brazil*

[b] *Department of Mechanical Engineering, Federal University of Santa Catarina, Florianópolis-SC, 88040-900, Brazil*

Received 7 January 2000; received in revised form 9 May 2001

Abstract

Heat and mass conservation equations in porous media are coupled and, in general, solved, iteratively, by using the values of temperature and moisture content from previous iteration to calculate source terms. This is the *traditional* mathematical method and numerical stability is only ensured for small time steps, depending on the source term's magnitudes. This is specially important, when material properties have *strong* variations with moisture content. This paper presents an unconditionally stable numerical method, conceived accordingly to a new methodology, which considers: (i) linearization of the term giving the vapor exchanged at the boundaries in terms of temperature and moisture content and (ii) introduction of a new generic algorithm to solve, *simultaneously*, the governing equations, for each time step. Numerical stability of these two methods are compared and it is shown that, in addition to avoid numerical unstability for arbitrary time steps and material properties, convergence is always quickly reached, in the presently proposed calculation method.

1. Introduction

In several fields such as drying processes, agriculture and building energy analysis, it is important to know the dynamics of temperature and moisture content distributions and how they are related to each other to evaluate heat flux and mass flow through porous media.

In spite of the main focus of this paper is on the presentation of a new mathematical method and show how it is applied in hygrothermal studies of porous building materials, the heat and mass transfer formulation presented can also be used in many other fields where the mass and energy balances are the governing equations.

In building energy analysis, calculated heat conduction through walls usually neglects the storage and transport of moisture in the porous structure of the walls. However, walls are normally submitted to both thermal and moisture gradients so that an accurate heat transfer determination requires a simultaneous calculation of both sensible and latent effects.

Besides its effect on heat transfer, moisture has other implications, especially in hot/humid climates. It is well known that moisture can cause damage to the building structure and can promote the growth of mold and mildew, affecting the health of building occupants.

Several investigators have developed models for moisture transport in porous materials. Cunningham [1] developed a mathematical model for hygroscopic materials in flat structures that uses an electrical analogy with resistances for the vapor flow and an exponential approximation function with constant mass transport coefficients. Keresteciogłu and Gu [2] investigated the phenomenon using evaporation–condensation theory in the pendular state (unsaturated liquid flow stage). The application of this theory is limited to low moisture content. Burch and Thomas [3] developed a computer

* Corresponding author. Tel.: +55-41-330-1322; fax: +55-41-330-1349.

E-mail address: nmendes@ccet.pucpr.br (N. Mendes).

0017-9310/02/$ - see front matter
PII: S0017-9310(01)00172-7

program, MOIST, using the finite-difference method to estimate the heat and mass transfer through composite walls under non-isothermal conditions. El Diasty et al. [4] used an analytical approach that assumed isothermal conditions and constant transport coefficients. Liesen [5] used evaporation–condensation theory and a response factor method to develop and implement a model of heat and mass transfer in the building thermal simulation program integrated building loads analysis and system thermodynamics (IBLAST). Hygrothermal property variations were neglected and liquid transfer was not considered. In this way, IBLAST is restricted to a very low moisture content, although requiring short calculation time. Yik et al. [6] developed a fast model integrated with air-conditioning system component models that employs evaporation–condensation theory with differential permeability. In fact, above-described models originated many simulation programs to predict the heat and moisture transfer through porous building walls, but using calculation methods that are *conditionally stable*.

As the present paper is focused on the numerical method rather than on heat and mass transfer model itself, a complete discussion about mathematical models was avoided. Actually, all those models have nearly the same origin (heat and mass balance equations, Philip and De Vries model and the laws of Fourier, Fick and Darcy). The main difference among them is related to the particular assumptions used. In this way, it is believed that the models are, generally, reliable and the main aspect that will be treated, here, is the calculation method itself.

In IEA Annex 24 [7], 5 models are commented in detail: 1D-HAM, WUFIZ, MATCH, HYGRAN24 and LATENITE. Below, they are briefly described in terms of their solvers.

1D-HAM models air flow (as a known flux), heat conduction and vapor diffusion. Time step depends on a stability criterion for the explicit forward differences scheme. The transport coefficients are assumed to be constant. WUFIZ matrix equations are solved per time step by using an alternating-direction implicit method (ADI), with iteration between heat and moisture until a desired accuracy is reached. It uses an implicit forward control volume method. ADI method is a commonly used line-by-line method, which was introduced by Peaceman and Rachford in 1955 [8]. HYGRAN24 models air flow, heat conduction and vapor and liquid diffusion. For each time step, air flow is, first, calculated. Then, heat and moisture matrix equations are solved consecutively, in an iterative loop, until the desired accuracy is reached. It uses Cranck–Nicholson scheme. LATENITE equations can be solved in either iterative or block form. A delta form is employed for the discontinuous set of strongly coupled equations. MATCH heat matrix equation is solved for each time step. Then moisture equation is solved in a two-step procedure. First, vapor pressure is calculated using suction pressure data of the previous step. Then, the new vapor pressure data are used as a known term, to calculate the new suction values. No iteration inside a time step is applied. In MATCH, the amount of vapor condensing or evaporating in the control volume is taken, explicitly, from the former time step and, according to what was stated by Pedersen [9], in some cases it may be relevant to let liquid moisture transport term out of the calculation. If this is not followed, the non-linearity of the problem would not guarantee the overall moisture balance to be kept.

This statement [9] shows that the algorithm used in MATCH may have unstability problems even if the source term (the amount of vapor condensing or evaporating in the control volume) is calculated from the former time step, which means that the source term is written as a constant for each time step so that no iteration is needed. In this way, unstability problems might appear because the solver does not, really, solve, simultaneously, the highly coupled governing equations.

MOIST [10] normally uses 1-h time step and provides reasonable results. However, the use of a such large time step for low density insulation materials may make MOIST simulations unstable and physically unrealistic. This shows that MOIST algorithm is not always stable and small time steps may be required to avoid numerical convergence problems.

In general, as it can be noticed by IEA Annex 24 description [7], by Pedersen [9] and by Burch and Chi [10], any of the codes, mentioned above, does not have an algorithm with such a robust solver to calculate simultaneously the temperature and moisture content distributions. Instead, they have stability criteria and time step control devices to reduce numerical convergence problems. In the present paper a new calculation method is presented, in order to enable yearly simulation of heat and moisture transfer in building porous walls, possible to be performed with reduced processing times, considering *arbitrary* material properties and boundary conditions. The method was conceived to preserve numerical stability as a result of two new considerations. The first considers the vapor exchanged between the wall surfaces and the air, as a linear function of temperature and moisture content, rather than vapor concentration. The second introduces a new generic algorithm to solve, *simultaneously*, the governing equations.

This new tridiagonal algorithm uses tensors instead of scalar numbers so that it reaches numerical convergence very quickly by solving, at the same iteration level, both equations together, independently of their coupling terms.

It is shown that the presently proposed method leads to reliable results, free of numerical-stability related problems.

2. Mathematical model

The governing partial differential equations to model heat and mass transfer through porous media are given by Eqs. (1) and (2). They were derived from conservation of mass and energy flow in a 1-D elemental volume of porous material. The energy conservation equation is written as

$$\rho_0 c_m(T,\theta)\frac{\partial T}{\partial t} = \frac{\partial}{\partial x}\left(\lambda(T,\theta)\frac{\partial T}{\partial x}\right) - L(T)\frac{\partial}{\partial x}(j_v), \tag{1}$$

while the mass conservation equation as

$$\frac{\partial \theta}{\partial t} = -\frac{\partial}{\partial x}\left(\frac{j}{\rho_l}\right), \tag{2}$$

where ρ is the solid matrix density, c_m, mean specific heat, T, temperature, t, time, λ, thermal conductivity, L, latent heat of vaporization ($= h_{LV}$), θ, volume basis moisture content, j_v, vapor flow, j, total flow and ρ_l the water density.

Note that Eq. (1) differs from Fourier's equation for transient heat flow by a source term due to phase change within the pores. According to Philip and DeVries [11], vapor flow density is given by

$$\frac{j_v}{\rho_l} = -D_{Tv}(T,\theta)\frac{\partial T}{\partial x} - D_{\theta v}(T,\theta)\frac{\partial \theta}{\partial x} \tag{3}$$

and for total mass flow density

$$\frac{j}{\rho_l} = -D_T(T,\theta)\frac{\partial T}{\partial x} - D_\theta(T,\theta)\frac{\partial \theta}{\partial x} \tag{4}$$

with $D_T = D_{Tl} + D_{Tv}$ and $D_\theta = D_{\theta l} + D_{\theta v}$, where D_{Tl} is the liquid phase transport coefficient associated to a temperature gradient, D_{Tv}, vapor phase transport coefficient associated to a temperature gradient, $D_{\theta l}$, liquid phase transport coefficient associated to a moisture content gradient, $D_{\theta v}$, vapor phase transport coefficient associated to a moisture content gradient, D_T, mass transport coefficient associated to a temperature gradient (m^2/s °C) and D_θ, mass transport coefficient associated to a moisture content gradient (m^2/s).

2.1. Boundary conditions

The associated conservation equations at the outside and inside wall surface are as follows. For the outside surface ($x = 0$), it was considered that the wall is exposed to short-wave radiation, convection heat and mass transfer, and phase change. Thus, the energy balance becomes

$$-\left(\lambda(T,\theta)\frac{\partial T}{\partial x}\right)_{x=0} - (L(T)j_v)_{x=0} = h(T_\infty - T_{x=0}) + \alpha q_r + L(T)h_m(\rho_{v,\infty} - \rho_{v,x=0}), \tag{5}$$

where $h(T_\infty - T_{x=0})$ represents the heat exchanged with the outside air, described by the surface conductance h, αq_r is the absorbed short-wave radiation and $h_m(\rho_{v,\infty} - \rho_{v,x=0})$, the phase change energy term. The solar absorptivity is defined as α and the mass convection coefficient as h_m which is related to h by Lewis' relation.

The mass balance at the outside surface ($x = 0$) is described as

$$-\frac{\partial}{\partial x}\left(D_\theta(T,\theta)\frac{\partial \theta}{\partial x} + D_T(T,\theta)\frac{\partial T}{\partial x}\right)_{x=0} = \frac{h_m}{\rho_l}(\rho_{v,\infty} - \rho_{x=0}). \tag{6}$$

The same above equations apply to the inside surface ($x = L$), with the omission of short-wave related terms.

3. The traditional heat and mass transfer calculation method

The governing equations are discretized by using the control-volume formulation method. The interpolation method used in this 1-D problem is the central-difference scheme (CDS).

Due to coupling between moisture content θ and temperature T, Eqs. (1)–(4) are, as usually, discretized in the form given below. For internal points, the mass conservation equation is written as

$$\left(\frac{\Delta x}{\Delta t} + \frac{D_{\theta e}}{\delta x_e} + \frac{D_{\theta w}}{\delta x_w}\right)\theta_P = \frac{D_{\theta e}}{\delta x_e}\theta_E + \frac{D_{\theta w}}{\delta x_w}\theta_W + \frac{\Delta x}{\Delta t}\theta_P^o + \left[\frac{D_{Te}}{\delta x_e}(T_E^o - T_P^o) - \frac{D_{Tw}}{\delta x_w}(T_P^o - T_W^o)\right] \tag{7}$$

and the energy conservation equation is written as,

$$\left(\rho_0 c_m\frac{\Delta x}{\Delta t} + \frac{\lambda_e}{\delta x_e} + \frac{L\rho_l D_{Tve}}{\delta x_e} + \frac{\lambda_w}{\delta x_w} + \frac{L\rho_l D_{Tvw}}{\delta x_w}\right)T_P = \left(\frac{\lambda_e}{\delta x_e} + \frac{L\rho_l D_{Tve}}{\delta x_e}\right)T_E + \left(\frac{\lambda_w}{\delta x_w} + \frac{L\rho_l D_{Tvw}}{\delta x_w}\right)T_W + \rho_0 c_m\frac{\Delta x}{\Delta t}T_P^o + L\rho_l\left(\frac{D_{\theta ve}(\theta_E^o - \theta_P^o)}{\delta x_e} - \frac{D_{\theta vw}(\theta_P^o - \theta_W^o)}{\delta x_w}\right), \tag{8}$$

where superscript "o" indicates that the variable assumes its previous value. Subscripts p, e(E) and w(W) are related, as usually, to node p and its neighbors at east and west side, respectively.

In the same way, Eqs. (5) and (6) are put in discrete form to obtain the following expressions for the half-volume node at the boundaries ($S = 0, L$):

$$\left(\frac{\Delta x}{2\Delta t}+\frac{D_{\theta e}}{\delta x_e}\right)\theta(S)=\frac{D_{\theta e}}{\delta x_e}\theta(n(S))+\frac{\Delta x}{2\Delta t}\theta^o(S)+D_{Te}\left(\frac{T^o(n(S))-T^o(S)}{\delta x_e}\right)+\frac{h_{mt}}{\rho_l}(\rho_{v,\infty}-\rho(S)) \quad (9)$$

and

$$\left(\rho_0 c_m\frac{\Delta x}{2\Delta t}+\frac{\lambda_e}{\delta x_e}+L\rho_l\frac{D_{Tve}}{\delta x_e}+h\right)T(S)=\left(\frac{\lambda_e}{\delta x_e}+L\rho_l\frac{D_{Tve}}{\delta x_e}\right)T(n(S))+\rho_0 c_m\frac{\Delta x}{2\Delta t}T^o(S)+L\rho_l D_{\theta ve}\left[\frac{\theta^o(n(S))-\theta^o(S)}{\delta x_e}\right]+hT_\infty.+\alpha(1-\delta(S,L))q_r+Lh_m(\rho_{v,\infty}-\rho_v(S)). \quad (10)$$

where $n(S)$ is the internal point neighbor to S and $\delta(a,b)$ is the Kronecker delta ($\delta(a,b)=1$ for $a=b$ and 0 otherwise).

Eqs. (7)–(10) have the form

$$A_P\Phi_P=A_E\Phi_E+A_W\Phi_W A_P^o\Phi_W+D, \quad (11)$$

where $A_P=A_E+A_W+A_P^o$, $D=A_P^o\Phi_P^o+F$ and Φ is a dependent variable (T or θ).

The source term D contains – besides the transient term ($A_p^o\Phi_p^o$) – all the terms $\rho_v(S)=\rho_v(\theta,T)$ which are non-linear functions of the dependent variables. As the solution method is iterative, the values calculated for T and θ from the previous iteration are used for calculating the source terms in the above equations. In this traditional method, mass and energy conservation equations are thus *uncoupled*, as coupling terms are always evaluated at a previous iteration.

3.1. Stability conditions

Linearized Eqs. (7)–(10) can be seen as two uncoupled tridiagonal system of equations – one for T and the other for θ, where the main diagonal is given by the coefficients that accompany Φ_P – Eq. (11).

Decoupling of heat and mass conservation equations results in high magnitude source terms, which are added to the non-linear surface terms, associated to $\rho_v(\theta,T)$ dependence. Linear systems of equations are numerically solvable when main diagonal terms are dominant. It is, thus, suitable that the source term in Eq. (11) be dismembered in way to decrease its magnitude and increase the main diagonal – terms A_p. In the present case, positiveness of vapor concentration difference ($\rho_{v,\infty}-\rho_v(S)$), at a given step, means a given amount of vapor condensing on the surface and may raise, substantially, the surface moisture content and temperature, producing vapor flow inversion. This unphysical, flow inversion occurs because the mass flow resistance towards the opposite side of the wall is higher and can happen continuously for high time steps, preventing the solution to converge. Therefore, for the traditional method, numerical stability is only ensured for very small time steps.

To solve the stability problem and to increase the time step, vapor concentration difference was linearized in terms of temperature and moisture content differences to strengthen the main diagonal. Linearization is discussed in the following section.

4. Mathematical considerations for the vapor exchanged between the wall surfaces and air

Vapor flow between a porous surface and air is normally written as a function of vapor concentration difference – $\Delta\rho_v$ – which requires vapor flow to be evaluated with previous values of temperature and moisture content. In this way, it is, in general, included in the source term of the system of equations, giving additional unstablity source terms.

It is described below a new procedure to calculate vapor flow, independently of previous values of temperature and moisture content by writing $\Delta\rho_v$ as a linear combination of temperature and moisture concentration difference.

The first assumption is that water vapor behaves like a perfect gas so that the concentration difference can be written as

$$(\rho_{v,\infty}-\rho_v(s))=\frac{P_\infty M}{\Re T_\infty}-\frac{P(s)M}{\Re T(s)}, \quad (12)$$

where $\Re$ is the universal gas constant, and M, the molecular mass.

Replacing the vapor pressure by the product $P_s\phi$ of saturated pressure P_s and relative humidity ϕ,

$$(\rho_{v,\infty}-\rho_v(s))=\frac{P_{s,\infty}\phi_\infty M}{\Re T_\infty}-\frac{P_s(s)\phi(s)M}{\Re T(s)}. \quad (13)$$

Eq. (13) can also be written as

$$(\rho_{v,\infty}-\rho_v(s))=\frac{M}{\Re}\left[\frac{P_{s,\infty}\phi_\infty}{T_\infty}+\frac{P_s(s)\phi_\infty}{T(s)}-\frac{P_s(s)\phi_\infty}{T(s)}-\frac{P_s(s)\phi(s)}{T(s)}\right], \quad (14)$$

or,

$$(\rho_{v,\infty}-\rho_v(s))=\frac{M}{\Re}\phi_\infty\left(\frac{P_{s,\infty}}{T_\infty}-\frac{P_s(s)}{T(s)}\right)+\frac{M}{\Re}\frac{P_s(s)}{T(s)}[\phi_\infty-\phi(s)], \quad (15)$$

At this point, the vapor concentration difference is written as a linear combination of relative humidity difference and the difference between the quotient of

saturation pressure by temperature. This quotient can be calculated by a first-degree function with small errors for a certain range of temperatures. For increasing accuracy, this is performed, introducing a residual function, $R(T)$, related to temperature as

$$R(T) = \frac{P_s}{T} - (AT + B), \tag{16}$$

where A and B are the straight-line coefficients from the approximation $P_s/T = AT + B$. The ratio P_s/T is calculated by the saturation pressure expression from ASHRAE [12].

Therefore, the difference between pressure and temperature quotients of Eq. (17) may be written as

$$\frac{P_{s,\infty}}{T_\infty} - \frac{P_s(s)}{T(s)} = A[T_\infty - T(s)] + R(T_\infty) - R(T(s)). \tag{17}$$

Similarly, it is possible to define a residual function related to moisture content difference – $R(\theta^{\text{prev}}(s))$, – then the term associated to the relative humidity of Eq. (15), is redefined as

$$\frac{M}{\Re}\frac{P_s(s)}{T(s)}[\phi_\infty - \phi(s)] = \frac{M}{\Re}\left(\frac{P_s(s)}{T(s)}\right)^{\text{prev}} \times \left[\frac{\partial\phi}{\partial\theta}(\theta_\infty - \theta(s)) + R(\theta^{\text{prev}}(S))\right], \tag{18}$$

where the $R(\theta_0^{\text{prev}})$ is the residue calculated by the sorption isotherm, evaluated at the previous iteration.

In this way, the above equation gives

$$\frac{M}{\Re}\left(\frac{P_s(s)}{T(s)}\right)[\phi_\infty - \phi(s)] = \frac{M}{\Re}\left(\frac{P_s(s)}{T(s)}\right)^{\text{prev}}\left(\frac{\partial\phi}{\partial\theta(s)}\right)^{\text{prev}}(\theta_\infty - \theta(s)) + \frac{M}{\Re}\left(\frac{P_s(s)}{T(s)}\right)^{\text{prev}} R(\theta^{\text{prev}}(S)). \tag{19}$$

Finally, replacing Eqs. (17) and (19) in the vapor concentration difference expression

$$(\rho_{v,\infty} - \rho_v(s)) = M_1(T_\infty - T(s)) + M_2(\theta_\infty - \theta(s)) + M_3, \tag{20}$$

where

$$M_1 = A\frac{M}{\Re}\phi, \quad M_2 = \frac{M}{\Re}\left(\frac{P_s(s)}{T(s)}\right)^{\text{prev}}\left(\frac{\partial\phi}{\partial\theta(s)}\right)^{\text{prev}},$$

$$M_3 = \frac{M}{\Re}\left[\left(\frac{P_s(s)}{T(s)}\right)^{\text{prev}} R(\theta^{\text{prev}}(s)) + \phi_\infty(R(T_\infty) - R(T^{\text{prev}}((s)))\right].$$

However, the influence of the previous iteration is still expressive, since there are temperature terms in the mass conservation equation and vice versa. This fact inspired a modification in the solution method, which was improved to calculate, simultaneously, the temperature and moisture content profiles. This is shown in the following section.

5. A generic algorithm to solve highly coupled governing equations

The development of a generic algorithm, to solve heat and mass transfer coupled equations, emerged from the need of obtaining all the dependent variable profiles simultaneously at a given time step avoiding numerical divergence caused by the evaluation of coupled terms from previous iteration values. In this way, the method becomes stable and closer to the nature of the physical phenomenon of combined heat and mass transfer in porous media.

Discretization of conservation equations in the physical domain gives the following algebraic equations:

$$\mathbf{A}_i \cdot \mathbf{x}_i = \mathbf{B}_i \cdot \mathbf{x}_{i+1} + \mathbf{C}_i \cdot \mathbf{x}_{i-1} + \mathbf{D}_i, \tag{21}$$

where $\mathbf{x}$ is a vector containing the dependent variables. In the present case

$$\mathbf{x}_i = \begin{bmatrix} \theta_i \\ T_i \end{bmatrix} \tag{22}$$

and, differently from the traditional TDMA, coefficients A, B and C are the second-order tensors. Vector $\mathbf{x}_i$ can be expressed as a function of $\mathbf{x}_{i+1}$

$$\mathbf{x}_i = \mathbf{P}_i \cdot \mathbf{x}_{i+1} + \mathbf{q}_i, \tag{23}$$

where P_i is, now, a second-order tensor.

Replacing Eq. (23), evaluated at point $i-1$ in (21), the following equation is obtained:

$$(\mathbf{A}_i - \mathbf{C}_i \cdot \mathbf{P}_{i-1})\mathbf{x}_i = \mathbf{B}_i \cdot \mathbf{x}_{i+1} + \mathbf{C}_i \cdot \mathbf{q}_{i-1} + \mathbf{D}_i. \tag{24}$$

Writing Eq. (24) in an explicit way for $\mathbf{x}_i$

$$\mathbf{x}_i = \left[(\mathbf{A}_i - \mathbf{C}_i \cdot \mathbf{P}_{i-1})^{-1} \cdot \mathbf{B}_i\right] \cdot \mathbf{x}_{i+1} + (\mathbf{A}_i - \mathbf{C}_i \cdot \mathbf{P}_{i-1})^{-1}(\mathbf{C}_i \cdot \mathbf{q}_{i-1} + \mathbf{d}_i). \tag{25}$$

Thus, a comparison between Eqs. (25) and (23) gives the following new recursive expressions:

$$\mathbf{P}_i = \left[(\mathbf{A}_i - \mathbf{C}_i \cdot \mathbf{P}_{i-1})^{-1} \cdot \mathbf{B}_i\right] \tag{26}$$

and

$$\mathbf{q}_i = (\mathbf{A}_i - \mathbf{C}_i \cdot \mathbf{P}_{i-1})^{-1}(\mathbf{C}_i \cdot \mathbf{q}_{i-1} + \mathbf{D}_i). \tag{27}$$

The use of this new algorithm is illustrated in the sections below, by developing the new mathematical method.

6. The new heat and mass transfer calculation method

The new method was derived from the traditional one by using the new algorithm and the linearization of vapor concentration difference, to solve simultaneously the governing equations on a very stable way. Thus, for this new method, the coefficients for internal points are:

$$
\begin{aligned}
A(i) &= \begin{bmatrix} \frac{\Delta x}{\Delta t} + \frac{D_{\theta e}}{\delta x_e} + \frac{D_{\theta w}}{\delta x_w} & \frac{D_{Te}}{\delta x_e} + \frac{D_{Tw}}{\delta x_w} \\ L\rho_l\left(\frac{D_{\theta ve}}{\delta x_e} + \frac{D_{\theta vw}}{\delta x_w}\right) & \left(\frac{\lambda_e}{\delta x_e} + \frac{LD_{Tve}}{\delta x_e} + \frac{\lambda_w}{\delta x_w} + \frac{LD_{Tvw}}{\delta x_w} + \rho_0 c_m \frac{\Delta x}{\Delta t}\right) \end{bmatrix}, \\
B(i) &= \begin{bmatrix} \frac{D_{\theta e}}{\delta x_e} & \frac{D_{Te}}{\delta x_e} \\ L\rho_l \frac{D_{\theta ve}}{\delta x_e} & \left(\frac{\lambda_e}{\delta x_e} + \frac{LD_{Tve}}{\delta x_e}\right) \end{bmatrix}, \\
C(i) &= \begin{bmatrix} \frac{D_{\theta w}}{\delta x_w} & \frac{D_{Tw}}{\delta x_w} \\ L\rho_l \frac{D_{\theta vw}}{\delta x_w} & \left(\frac{\lambda_w}{\delta x_w} + \frac{LD_{Tvw}}{\delta x_w}\right) \end{bmatrix}, \\
D(i) &= \begin{bmatrix} \frac{\Delta x}{\Delta t}\theta_P^o \\ \rho_0 c_m \frac{\Delta x}{\Delta t} T_P^o \end{bmatrix}
\end{aligned}
\tag{28}
$$

and for the boundary volume S,

$$
\begin{aligned}
A(S) &= \begin{bmatrix} \frac{\Delta x}{2\Delta t} + \frac{D_{\theta e}}{\delta x_e} + M_2 \frac{h_m}{\rho_l} & \frac{D_{Te}}{\delta x_e} + M_1 \frac{h_m}{\rho_l} \\ \frac{L\rho_l D_{\theta ve}}{\delta x_e} + LM_2 h_m & \rho_0 c_m \frac{\Delta x}{2\Delta t} + \frac{\lambda_e}{\delta x_e} + \frac{L\rho_l D_{Tve}}{\delta x_e} + h + LM_1 h_m \end{bmatrix}, \\
B(S) &= \begin{bmatrix} \frac{D_{\theta e}}{\delta x_e} & \frac{D_{Te}}{\delta x_e} \\ \frac{L\rho_l D_{\theta ve}}{\delta x_e} & \left(\frac{\lambda_e}{\delta x_e} + \frac{L\rho_l D_{Tve}}{\delta x_e}\right) \end{bmatrix}, \\
C(S) &= \begin{bmatrix} 0 & 0 \\ 0 & 0 \end{bmatrix}, \\
D(S) &= \begin{bmatrix} \frac{h_m}{\rho_l}(M_1 T_\infty + M_2 \theta_\infty + M_3) + \frac{\Delta x}{2\Delta t}\theta^o(S) \\ hT_\infty + \alpha(1 - \delta(S,L))q_r + Lh_m(M_1 T_\infty + M_2 \theta_\infty + M_3) + \rho_0 c_m \frac{\Delta x}{2\Delta t} T^o(S) \end{bmatrix}.
\end{aligned}
\tag{29}
$$

This new method is much less dependent on the T and θ fields of the previous iteration. Nevertheless, it is still necessary to make iterations because transport coefficients and residues are calculated by using the previous T and θ fields. However, this does not have any significant influence on the solution of the system of equations by the new mathematical method.

7. Results

7.1. Material properties

In order to show the numerical performance of the proposed method, material property data are provided for simulating building walls that are largely used in hot and humid countries.

The basic dry-basis material properties are given in Table 1. In this table *open porosity* is the ratio of the volume of open pores (i.e., pores with openings that have a path to both wall surfaces) to the total volume.

The available material data gathered from Perrin [15] allow all the transport coefficients to be modeled as a function of moisture content. Figs. 1–3 show the property data for lime mortar as a function of moisture content. Considering the temperature range of interest in building applications, temperature dependence of lime mortar properties was, here, neglected when compared to their dependence with moisture content.

In Fig. 1, vapor and total (liquid plus vapor) transport coefficients for lime mortar are shown.

Table 1
Dry-basis material properties for lime mortar

ρ_0 (kg/m^3)	2050.0
λ (W/m K)	1.96
c_m (J/kg K)	950.0
Open porosity	0.18

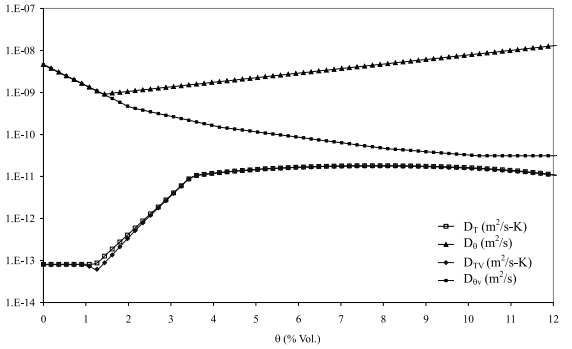

Fig. 1. Mass transport coefficients for lime mortar.

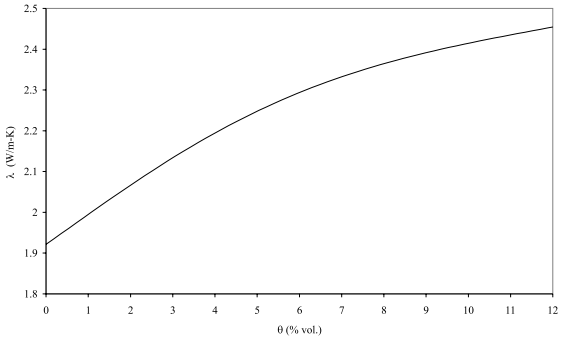

Fig. 2. Thermal conductivity for lime mortar.

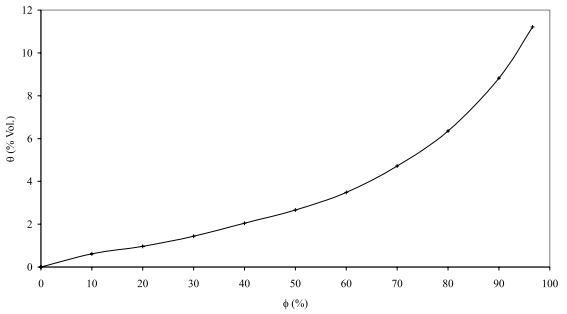

Fig. 3. Sorption isotherm curve for lime mortar.

It is possible to see from Fig. 1 that the coefficient responsible for the flow of liquid due to a temperature gradient (D_{Tl}) is very small compared to the one for vapor since the differences between the curves of D_T and D_{Tv} are very small.

Fig. 2 presents the thermal conductivity curves for both materials. In these curves, the vapor diffusion and phase change effects were not considered, which means that they show the value for pure thermal conductivity for heat transfer conduction in Fourier's law.

Fig. 3 presents the sorption isotherm curve for lime mortar. This curve is the average between adsorption and desorption curves.

7.2. Simulation results: comparative analysis

Comparative studies between the traditional and the new methods are presented. First, the influence of dimensionless numbers on the stability of the traditional method is analyzed. Then, comparisons are made in terms of vapor flow, temperature, moisture content, heat flux and time averaged heat flux through a porous building wall for both methods. At the end of this section, the influence of high time-step on the performance of the new method is described.

7.2.1. Dimensionless numbers influence

A dimensionless number that could numerically express when numerical instability arises is the Biot number for moisture diffusion (Bi_m). This number can be written as

$$Bi_m = \frac{h_m L}{D_\theta},$$

which means, for high Bi_m numbers, that wall higric resistance is much higher than the corresponding surface resistance.

Another important dimensionless number is the mass Fourier number, $Fo_m = D_\theta \Delta t/\Delta x^2$, expressing a mesh-size parameter that could be related to a convergence error function δ, defined as the relative difference between the wall surface moisture content values

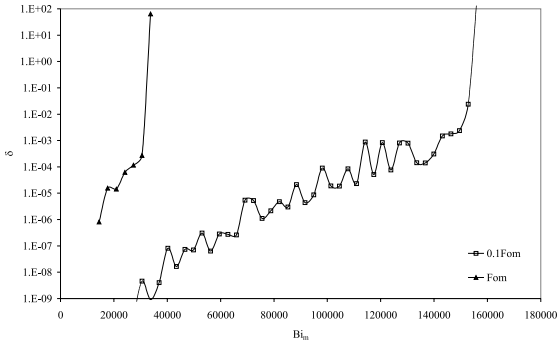

Fig. 4. Convergence error as a function of Bi_m, for $Fo_m = 7e-4$.

$$\delta = \mathrm{abs}\left(\frac{\theta_s - \theta_s^{prev}}{\theta_s^{prev}}\right).$$

Fig. 4 illustrates the influence of the Biot and Fourier numbers on the convergence error function.

It is noted, for the traditional method, as the Bi_m increases the error function goes up very quickly showing a high sensitivity to this dimensionless number, which can be even higher than that caused by the mass Fourier number.

The mass conservation equation at the boundaries can be written as

$$\left(\frac{1}{2Fo_m}+1\right)\theta(s) = \theta(s+1) + \frac{\theta^{Ant}(s)}{2Fo_m} + \mathrm{Bi}_m \frac{(\rho_{v,\infty} - \rho_v(s))}{\rho_l} - \frac{D_T}{D_\theta}(T^{prev}(s) - T^{prev}(1)).$$

The system of equations is stable when the left-hand term is much higher than the source terms (from the 2nd to the 4th right-hand terms). The last right-hand term is normally lower than the 2nd and 3rd ones. As the second right-hand term is comparable to the first parcel at the right-hand side of the equation above, it is believed that a good stability criterion, dependent on the boundary condition, but independent on the Fourier number, could be proposed as

$$Bi_m \frac{(\rho_{v,\infty} - \rho_v(s))}{\rho_l} \ll 1,$$

which can be satisfied for materials with high D_θ or for very low permeation surfaces, under any boundary condition value. However, as it can be seen in Fig. 4, the higher the Fo_m number the lower the Bi_m number to avoid numerical divergence.

7.2.2. Comparison between the traditional and the new methods

In order to illustrate the vapor flow inversion problem and the advantages of the new method, a symmetric

problem was firstly studied, when a lime mortar wall, initially with a moisture content of 3% in volume and temperature 20°C, was put in contact with air at a temperature of 28°C and 80%, at both wall surfaces. Solar radiation was ignored. Considering its equilibrium value, average wall moisture content increases monotonically, with time, toward its equilibrium value.

Fig. 5 shows, at the very beginning of the simulation, in the first time step, the vapor flow at the surfaces of a 100-mm lime mortar wall for each iteration. Three iterations were needed, in the new method, to reach convergence. However, for the traditional method, convergence was not reached since the Fo_m and Bi_m numbers were too high to avoid numerical divergence. This *non-physical* behavior can be explained by considering the numerical algorithm related to mass conservation equation, in *traditional* a method, that produces a very high quantity of moisture that comes to the wall surface. As the wall higric resistance is much higher than the air film resistance, moisture content at the surface increases substantially. In the sequence, energy balance equations are solved and the wall may lose energy to the air, especially if the source term was calculated with the new values of moisture content. If not, for the next iteration, the vapor concentration difference at the wall surface might be higher than that of the air, inverting vapor flow and preventing a stable solution.

Fig. 6 shows the same example illustrated in Fig. 5, for a 30-s time step. In this case, both models behave similarly showing a difference of 0.126% for the 1st iteration. After the third iteration, this difference remained constant at the value of 0.032%, which is very satisfactory.

Therefore, the traditional method can only be used for small time steps or small Fo_m numbers. The Fourier mass number decreased 125 times from the one used for Fig. 5 to that for Fig. 6, allowing convergence for the same Bi_m number. Actually, this is what many conditionally stable method programs do to avoid divergence problems or even physically unrealistic solutions.

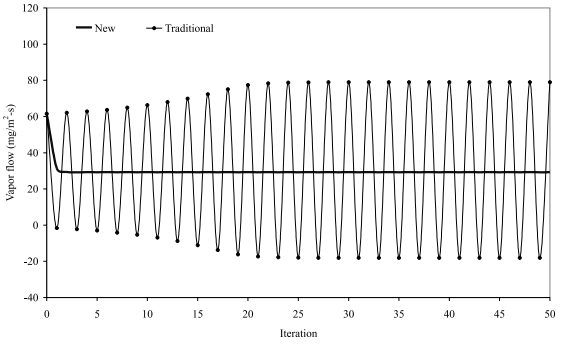

Fig. 5. Vapor flow at the surfaces of a 100-mm lime mortar wall for 1-h time step.

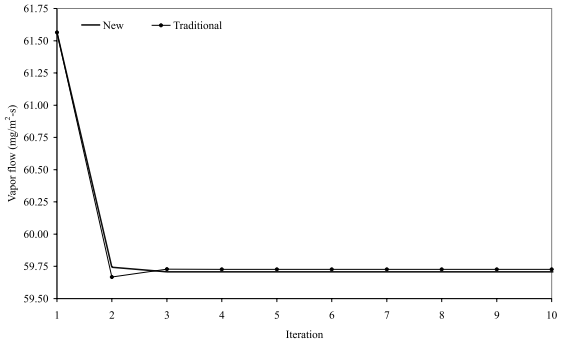

Fig. 6. Vapor flow at the surfaces of a 100-mm lime mortar wall for 30-s time step.

In Fig. 6, a good agreement for vapor flow calculation by both methods is also indicated when a 30-s time step is used. Nonetheless, by looking at the second iteration, it is remarkable that the new method still shows a better numerical performance.

As material properties vary significantly with moisture content and residual functions are calculated with previous iteration values of temperature and moisture content, it is necessary to make at least a single iteration when the new method is used, however convergence is rapidly achieved.

Fig. 7 displays the temperature at the wall surface. It is noticed, for a high time step, high fluctuations with the traditional method even for temperature, due to the latent term in the energy balance at the boundaries. It is perceived again that it would not be necessary to make more than three iterations by using the new method.

In Fig. 8, it is shown how the wall temperature distribution behaves for each iteration, at the very beginning of the simulation, with the new method. It is remarkable how fast convergence is attained, by using this method.

Fig. 9 presents the same temperature profiles, obtained by the traditional method. It can be observed that

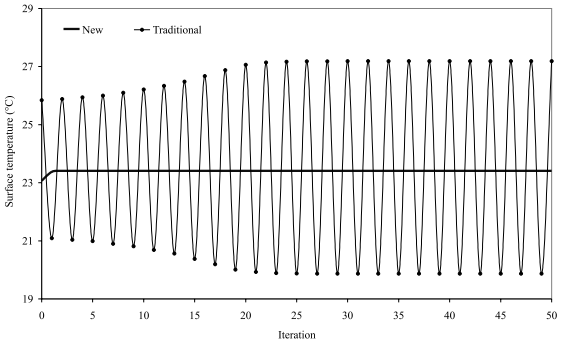

Fig. 7. Temperature at the surfaces of a 100-mm lime mortar wall for 1-h time step.

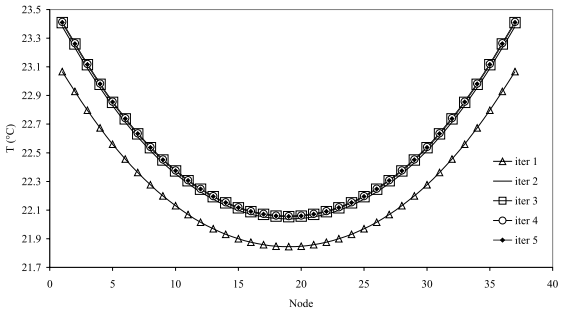

Fig. 8. Temperature profiles obtained by using the new method.

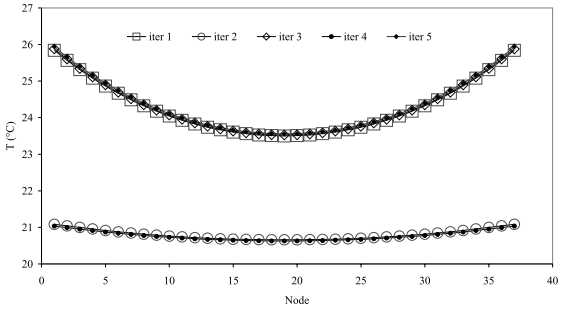

Fig. 9. Temperature profiles obtained by using the traditional method.

the temperature profile goes up and down at each iteration and does not stabilize. The even (or odd) iterations have about the same temperature profiles between themselves due to the vapor flow ''come-and-go'' problem.

Fig. 10 shows the evolution in time of temperature at the wall surfaces for both models with a 30 s time step. At each 50 iterations, a time step is incremented. In this case, it is noted that surface temperature evolution in time, for both models, is almost identical.

In conclusion, for high moisture diffusion Biot numbers and high time steps or high Fo_m numbers, the use of the traditional heat and moisture transfer calculation method will, likely, experience serious convergence problems.

Although, as was shown above, the new method allows to adopt any time step without numerical stability concerns, accuracy problems related to high time-step persist. In order to evaluate the errors associated to the time step magnitude, simulation results with the new method are presented for porous walls of air-conditioned buildings, in terms of heat flux. A 100-mm thick wall was simulated, without any additional mass flow resistance such as painting or vapor barriers, representing a critical situation for heat and moisture transfer.

The weather file used in the simulations was the Singapore Typical Meteorological Year (TMY). Data for solar radiation and internal psychrometric conditions were gathered from Mendes [13]. Internal temperature and relative humidity were obtained by using the DOE-2 building simulation program [14].

It was found for the temperature profiles on a very critical day of 14 January at 1:00 am (not shown) a largest difference of 0.7°C between simulations with time steps of 1 and 24 h.

Fig. 11 shows the differences on yearly integrated heat flux (sensible and latent) for the climate of Singapore, relative to 1-s time-step simulations. It is observed, in Fig. 11, that the use of 1-day time step gives a 10.9% difference when compared to the 1-s time-step simulation, which is very reasonable for estimating the initial conditions by a previous simulation. In fact, when a building porous envelope was simulated in Singapore with 24-h time step for the first year and 1-h time step for the second year, a difference of 0.05% was found in the calculation of integrated yearly heat flux, in comparison with simulations with 1 h time step for both years. It is, also, noticed that the use of time steps higher than 1 h would be suitable in situations where hourly

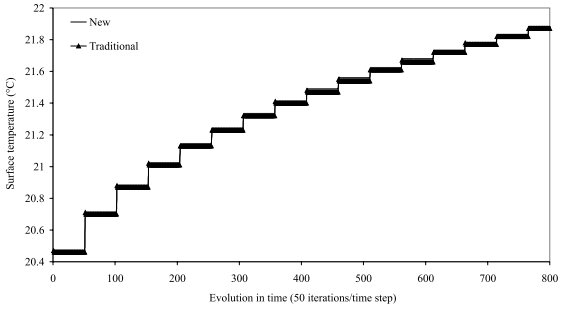

Fig. 10. Evolution in time of temperature at the surfaces of a lime mortar wall for a 30-s time step.

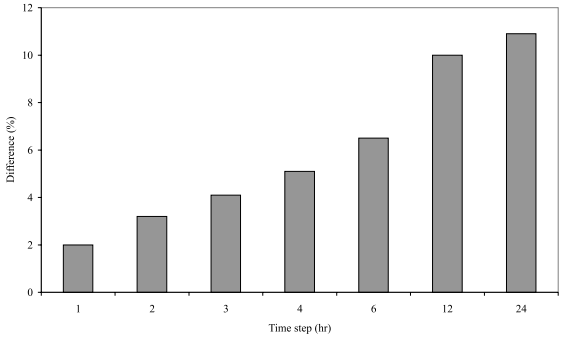

Fig. 11. Differences of yearly integrated heat flux calculation relative to 1-s time step simulations.

information is not needed or available and/or when computer running time plays an important role.

Therefore, it is easy to see that the use of 1-h time step simulations with the new method (unfeasible using the traditional one) allows to reach high accuracy, although with a computer running time reduction of nearly 1:3000.

8. Conclusions

Presently proposed method has shown a considerable progress when compared to traditional calculation methods, when a physical problem is described by strongly coupled equations.

The new method was applied to the problem of heat and moisture transfer through porous walls, by solving the governing equations, simultaneously and by considering the vapor exchanged between the wall and the air as a linear function of temperature and moisture content differences.

The use of this new method avoids numerical oscillations, since it keeps the discrete equations strongly coupled between themselves, preventing the occurrence of physically unrealistic behavior when time step is increased and producing an unconditionally-stable numerical method, which is very suitable to be used in building yearly energy simulation programs.

Acknowledgements

The authors thank CNPq – Conselho Nacional de Desenvolvimento Científico e Tecnológico – of the Secretary for Science and Technology of Brazil for support of this work.

References

[1] M.J. Cunningham, The moisture performance of framed structures: a mathematical model, Build. Environ. 23 (1988) 123–135.

[2] A. Keresteciogl u, L. Gu, Incorporation of the effective penetration depth theory into TRNSYS, Draft Report, Florida Solar Energy Center, Cape Canaveral, FL, 1989.

[3] D.M. Burch, W.C. Thomas, An Analysis of Moisture Accumulation in Wood Frame Wall Subjected to Winter Climate, NISTIR 4674, National Institute of Standards and Technology, Gaithersburg, 1991.

[4] R. El Diasty, P. Fazio, I. Budaiwi, Dynamic modeling of moisture absorption and desorption in buildings, Build. Environ. 28 (1993) 21–32.

[5] R.J. Liesen, Development of a response factor approach for modeling the energy effects of combined heat and mass transfer with vapor adsorption in building elements, Ph.D. Thesis, Mechanical Engineering Department, University of Illinois, Chicago, IL, 1994.

[6] F.W.H. Yik, C.P. Underwood, W.K. Chow, Simultaneous modeling of heat and moisture transfer and air-conditioning systems in buildings, in: Proceedings of the 4th IBPSA International Building Performance Simulation Association – Conference, Madison, WI, 1995.

[7] IEA (International Energy Agency) Annex 24 Final Report, Heat, Air, and Moisture Transfer in Insulated Envelope Parts, vol. 1, Task 1: Modelling, Belgium, 1996.

[8] S. Patankar, Numerical Heat Transfer and Fluid Flow, Hemisphere, New York, 1980.

[9] C.R. Pedersen, A transient model for analyzing the hygrothermal behavior of building constructions, building and simulation'91, in: Proceedings of the 3rd IBPSA International Building Performance Simulation Association – Conference, France, 1991.

[10] D.M. Burch, J. Chi, MOIST: A PC Program for Predicting Heat and Moisture Transfer in Building Envelopes, Release 3.0, NIST Special Publication 917, National Institute of Standards and technology, Gaithersburg, 1997.

[11] J.R. Philip, D.A. DeVries, Moisture movement in porous materials under temperature gradients, Trans. Amer. Geophys. Union 38 (2) (1957) 222–232.

[12] ASHRAE, ASHRAE Handbook – Fundamentals, American Society of Heating, Refrigerating and Air-Conditioning Engineers, Atlanta, 1993.

[13] N. Mendes, Models for prediction of heat and moisture transfer through porous building elements, Ph.D. Thesis, 225, Federal University of Santa Catarina (UFSC), Florianópolis, SC, Brazil, 1997 (in Portuguese).

[14] B.E. Birdsall, W.F. Buhl, K.L. Ellington, A.E. Erdem, F.C. Winkelmann, DOE-2 Basics version 2.1E, Energy and Environment Division, Lawrence Berkeley National Laboratory, University of California Berkeley, CA, 1994.

[15] B. Perrin, Etude des transferts couplés de chaleur et de masse dans des matériaux poreux consolidés non saturés utilisés en génie civil, Thèse Docteur d'Etat, Université Paul Sabatier de Toulouse, Toulouse, France, 1985.